Phosphoribosyl Anthranilate Isomerase Catalyzes a Reversible Amadori Reaction†

Ulrich Hommel,‡ Marc Eberhard,§ and Kasper Kirschner*

Abteilung Biophysikalische Chemie, Biozentrum der Universität Basel, Klingelbergstrasse 70, CH-4056 Basel, Switzerland

Received August 5, 1994; Revised Manuscript Received January 17, 1995®

ABSTRACT: Data from steady state and transient kinetics show that the functional phosphoribosyl anthranilate isomerase domain of the naturally bifunctional enzyme from *Escherichia coli* has properties similar to those of its artificially excised domain. The naturally monofunctional enzyme from *Saccharomyces cerevisiae* has significantly higher values of both k_{cat} and k_{cat}/K_M^{PRA}. The primary product of a single turnover of phosphoribosylanthranilate is fluorescent, but it slowly isomerizes to the nonfluorescent stable product. The latter is the competent substrate of indoleglycerol phosphate synthase, which catalyzes the subsequent step of tryptophan biosynthesis. The isomerization is characterized by a monoexponential decay independent of phosphoribosyl anthranilate isomerase. Due to a tentative assignment of the fluorescent, primary product and the nonfluorescent, stable product to an enol and a keto compound, respectively, tryptophan biosynthesis appears to be rate-limited by an uncatalyzed enol/keto tautomerization. A formal kinetic mechanism of the reaction catalyzed by phosphoribosyl anthranilate isomerase is proposed that is consistent with the combined enzymic and ligand binding properties of the three variants of phosphoribosyl anthranilate isomerase.

Phosphoribosyl anthranilate (PRA)[1] isomerase catalyzes the third step in the committed biosynthesis of tryptophan from chorismic acid, in which PRA is rearranged to CdRP: chorismate → anthranilate → PRA → CdRP → IGP → indole → tryptophan. The PRAI reaction is an intramolecular redox reaction (otherwise known as the Amadori rearrangement; Isbell & Frush, 1958). It involves elementary proton transfer steps and most likely leads to an enolamine as the first product (Scheme 1). The latter is thought to tautomerize to the α-amino ketone, which is the putative substrate for the subsequent enzyme, indoleglycerol phosphate synthase (IGPS; Walsh, 1979).

The structural organization of PRAI differs widely among microorganisms (Crawford, 1989). It is a monomer in *Saccharomyces cerevisiae* (Braus et al., 1988), but fused to the C-terminus of IGPS in *Escherichia coli* (Kirschner et al., 1980). The structure of this bifunctional enzyme has been solved by protein crystallography (Priestle et al., 1987) and subsequently refined to 2 Å resolution (Wilmanns et al., 1992). Interestingly, both PRAI and IGPS have the 8-fold βα-barrel (or TIM) fold, suggesting that they may have had

Scheme 1

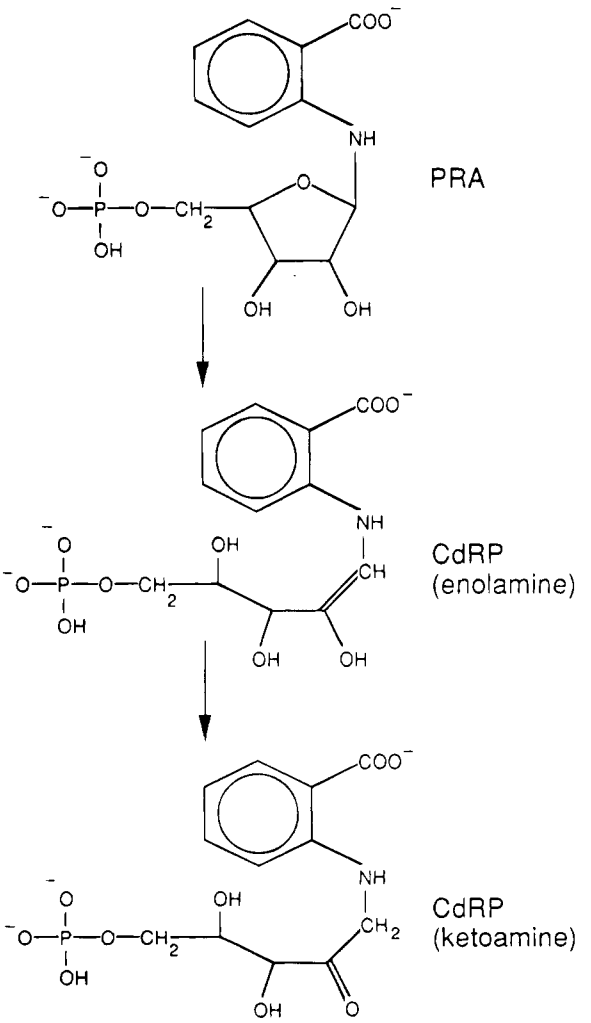

† This work was supported by Grant 3.255-1.85 from the Swiss National Science Foundation.

* Author to whom correspondence should be addressed.

‡ Present address: Sandoz Pharma AG, Lichtstrasse 35, CH 4002 Basel, Switzerland.

§ Present address: Department of Research, Cantonal Hospital, CH-4031 Basel, Switzerland.

® Abstract published in *Advance ACS Abstracts,* April 1, 1995.

[1] Abbreviations: PRA, *N*-(5′-phosphoribosyl)anthranilate; CdRP, 1-[(2-carboxyphenyl)amino]-1-deoxyribulose 5-phosphate; rCdRP, reduced CdRP; IGP, indoleglycerol phosphate; PRPP, 5′-phosphoribosyl 1-diphosphate; PRT, *N*-(5′-phosphoribosyl)anthranilate phosphoribosyltransferase (EC 2.4.2.18); PRAI, PRA isomerase or *N*-(5-phospho-β-D-ribosyl)anthranilate ketol-isomerase (EC 5.3.1.24); IGPS, IGP synthase or 1-[(2-carboxyphenyl)amino]-1-deoxy-D-ribulose 5-phosphate carboxylase (cycling) (EC 4.1.1.48); IGPS:PRAI, wild-type bifunctional enzyme from *Escherichia coli*; PRAI[ML256-452], engineered monofunctional variant of IGPS:PRAI (Eberhard et al., 1995); xPRAI, recombinant PRAI from *Saccharomyces cerevisiae* (Luger et al., 1989); IGPS[1-259], engineered monofunctional variant of IGPS:PRAI (Eberhard et al., 1995); EDTA, ethylenedinitrilo-*N*,*N*,*N*′,*N*′-tetraacetic acid; DTE, 1,4-dithioerythritol; GuCl, guanidinium chloride; HPLC, high-performance liquid chromatography.

0006-2960/95/0434-5429$09.00/0

a common ancestor (Farber & Petsko, 1990; Wilmanns et al., 1991). The bifunctional enzyme can be dissected at the genetic level into fully active monomeric proteins catalyzing either the PRAI or the IGPS reaction (Pflugfelder, 1986; Eberhard, 1990). Thus, three forms of PRAI are available: a recombinant version of the monomeric enzyme from *S. cerevisiae* expressed in *E. coli* (xPRAI; Luger et al., 1989), the excised monomeric domain (PRAI[ML256-452]; Eberhard et al., 1995), and the native, fused domain of the bifunctional enzyme from *E. coli* (IGPS:PRAI).

Here we describe the results of kinetic and ligand binding studies on the catalytic reaction of PRAI. The labile substrate PRA (Creighton, 1968) was synthesized in situ with the aid of anthranilate phosphoribosyltransferase (PRT; Hommel et al., 1989). The results lead to a plausible catalytic mechanism and suggest that a spontaneous enol/keto tautomerization may limit the overall rate of tryptophan biosynthesis.

EXPERIMENTAL PROCEDURES

Buffers. Buffer A: 0.05 M Tris-HCl (pH 7.5). Buffer B: 0.1 M Tris-HCl (pH 7.8) containing 5 mM EDTA and 2 mM DTE. Buffer C: 0.05 M Tris-HCl (pH 7.5) containing 4 mM K_2MgEDTA and 2 mM DTE.

Enzyme Purification. Purification of PRT (Hommel et al., 1989), xPRAI (Luger et al., 1989), PRAI[ML256-452] (Eberhard et al., 1995), IGPS[1-259] (Eberhard et al., 1995) and IGPS:PRAI (Kirschner et al., 1987) was performed as described.

Synthesis of Substrates and Inhibitors. PRA was synthesized enzymatically in situ as described (Eberhard et al., 1995). CdRP was synthesized either enzymatically or chemically and purified by reversed phase HPLC (Kirschner et al., 1987). rCdRP was synthesized by the reduction of CdRP according to Bisswanger et al. (1979).

Determination of Concentrations. The concentrations of anthranilate, CdRP, and rCdRP were determined spectrophotometrically by using the following extinction coefficients: anthranilate in buffer A, $\epsilon_{310} = 2.98\ mM^{-1}\ cm^{-1}$ and $\epsilon_{240} = 7.17\ mM^{-1}\ cm^{-1}$ (Doy & Gibson, 1959); rCdRP in 0.1 M potassium phosphate buffer at pH 7.0, $\epsilon_{327} = 3.43\ mM^{-1}\ cm^{-1}$ (Bisswanger et al., 1979). CdRP was quantified spectrophotometrically by complete conversion to IGP catalyzed by IGPS[1-259], using $\Delta\epsilon_{327} = 3.43\ mM^{-1}\ cm^{-1}$ and $\Delta\epsilon_{278} = 4.48\ mM^{-1}\ cm^{-1}$ (Creighton & Yanofsky, 1970). The concentration of PRPP was determined as described (Hommel et al., 1989). The concentration of IGPS:PRAI, IGPS[1-259], PRAI[ML256-452], and xPRAI were determined spectrophotometrically (Eberhard et al., 1995).

Steady State Kinetics. Steady state kinetics of PRAI was measured using enzymatically produced PRA (Hommel et al., 1989). PRA was generated in buffer C at 25 °C by the quantitative reaction of anthranilate with excess PRPP in the presence of 2 munits of PRT. One unit of activity is defined as the amount of enzyme that catalyzes the conversion of 1 μmol of substrate per minute to products at 25 °C under assay conditions. Fluorescence measurements were performed with a Perkin-Elmer 650-10S spectrofluorimeter interfaced via an analog-to-digital converter (PC-28 from Instrumatic AG, Switzerland) to a microcomputer (Twix 88-XT personal computer). Slits (2 nm) were used for both excitation and emission. Initial velocities at different substrate concentrations were evaluated with the direct linear plot method (Eisenthal & Cornish-Browden, 1974). Entire progress curves obtained under steady state conditions were evaluated by a nonlinear least-squares fit procedure according to the following rate equation (Fernley, 1974):

$$\frac{dx}{dt} = \frac{V_{max}}{1 + K_M^{PRA}/([PRA]_0 - x)} \quad (1)$$

where x is the concentration of CdRP, $[PRA]_0$ is the initial concentration of PRA, K_M^{PRA} is the Michaelis constant, and V_{max} is the maximal velocity. Competitive product inhibition was analyzed by fitting progress curves to the following rate equation (Duggleby & Morrison, 1977):

$$\frac{dx}{dt} = \frac{V_{max}}{1 - K_M^{PRA}/K_M^{CdRP} + K_M^{PRA}(1 + [S]_0/K_M^{CdRP})/([S]_0 - x)} \quad (2)$$

K_M^{CdRP} represents the product inhibition constant, which is identical to the Michaelis constant of the reverse reaction (CdRP → PRA; cf. Appendix). Progress curves were monitored with initial PRA concentrations between half and twice the value the K_M (Nimmo & Atkins, 1974). The addition of 32 munits of IGPS[1-259] (catalyzing the reaction CdRP → IGP; Eberhard et al., 1995) was required to convert CdRP rapidly to IGP and thereby to abolish product inhibition of PRAI completely. Progress curves were digitized for 50−100 time points by means of either a Hewlett-Packard 7440 plotter or on-line data aquisition. The data were analyzed with a least-squares fit program (Eberhard, 1990b).

The reverse reaction (CdRP → PRA) was followed either spectrophotometrically (using a Hewlett-Packard 8452A diode array instrument) or fluorometrically (by means of a Perkin-Elmer 650-10S spectrofluorimeter). Proteins were removed from enzymatically prepared CdRP by ultrafiltration (Centricon C-10). The reverse reaction was started by adding PRAI to solutions of CdRP and followed by recording either absorbance spectra (240−400 nm) or fluorescence excited at 310 nm. Data were evaluated as described under Results.

Kinetics of Ligand Binding and Single-Turnover Experiments. Stopped-flow measurements were performed in buffer C at 25 °C using the equipment described by Paul et al. (1980). The dead-time of the instrument was 1.7 ms at a driving pressure of 7 bar. Experimental data were analyzed on a Twix 88-XT computer by means of nonlinear least-squares fitting (Marquardt, 1963; Eberhard, 1990b). PRA fluorescence was excited at 313 nm (mercury line) and collected above 400 nm by means of a cutoff filter (Schott, Mainz). Protein fluorescence was excited at 280 nm and observed using a bandpass filter (330−380 nm). Fluorescence energy transfer from protein to bound rCdRP was observed by excitation at 280 nm and emission collection above 420 nm by means of a cutoff filter. Single-turnover experiments were performed with a constant molar ratio (10) of enzyme to substrate. PRA was prepared enzymatically in 2−3 mL portions as described earlier and used within 30 min. Individual progress curves (5−20) were averaged and fitted to single or double exponentials by nonlinear least-squares procedures (Marquardt, 1963; Eberhard, 1990b).

Progress curves of ligand binding were evaluated as described (Eberhard et al., 1995). Since both exponentials and progress curves represent nonlinear models, formal standard errors of their parameters cannot be derived from the equations; the distribution of parameters is non-Gaussian. Therefore, no standard deviations are given in the tables. None of the rate constants, dissociation constants, or steady state parameters determined in a series of identical experiments exhibited a variation of more than a factor of 2 (not shown).

Multiple-Mixing Experiments. Multiple-mixing, stopped-flow measurements were performed using an SFM-3 stopped-flow module (Biologic, France) composed of three stepping motor-driven syringes, an MPS 5/3 power supply, a 150 W xenon−mercury light source, a monochromator, and two photomultipliers, each equipped with a power supply and a signal amplifier. The BIOKINE software package (Biologic, France) running on a Tandon 486-AT computer was used for data acquisition and evaluation. All measurements were performed with a TC-100/15 cuvette (light path, 10 mm) supplied by Biologic. The flow rate was kept below 12 mL/s in order to avoid artifacts due to cavitation. All multiple-mixing experiments were performed in buffer C at 25 °C.

Determination of CdRP Fluorescence. CdRP was converted to IGP by the addition of IGPS[1-259]. The reaction was followed fluorimetrically (excitation at 310 nm, where anthranilate, PRA, and CdRP absorb, but IGP does not) by emission at 400 nm (Hankins et al., 1975). The amplitude of the remaining signal was compared to the fluorescence intensity of known concentrations of anthranilate and PRA. The percentages of contaminating anthranilate and PRA present in the preparation of CdRP were determined by conversion of these compounds to CdRP after further addition of PRPP, PRT, and PRAI and found to be less than 0.5% of the CdRP concentration.

RESULTS

Steady State Kinetics of the Forward PRAI Reaction. Since the spontaneous reaction of ribose 5-phosphate and anthranilate leads to CdRP via PRA (Creighton, 1970), the equilibrium appears to favor CdRP over PRA. Therefore, we first analyzed the kinetics of the PRAI reaction in the forward direction. Because the fluorescence quantum yield of PRA is 50-fold larger than that of CdRP (Doy, 1966; Hommel et al., 1989), it is convenient to use the disappearance of the fluorescence of PRA as a signal and to evaluate entire progress curves rather than only initial velocities. To ensure that PRA is consumed completely and that product inhibition by CdRP does not occur, we included an excess of IGPS[1-259] (Pflugfelder, 1986; Eberhard et al., 1995) that catalyzes the virtually irreversible conversion of CdRP to IGP.

Figure 1 illustrates a typical progress curve, obtained in this case with xPRAI, a monomeric variant of PRAI from *S. cerevisiae* (Luger et al., 1989). It shows that the linear part of the reaction proceeds for a longer time in the presence of excess IGPS. Because IGPS catalyzes the conversion of CdRP to IGP, the prolongation of the linear part must be due to the removal of the inhibiting product, CdRP. As shown in the following, the residual fluorescence observed in the absence of IGPS is due to a mixture of a fluorescent and a nonfluorescent isomer of CdRP. Addition of IGPS,

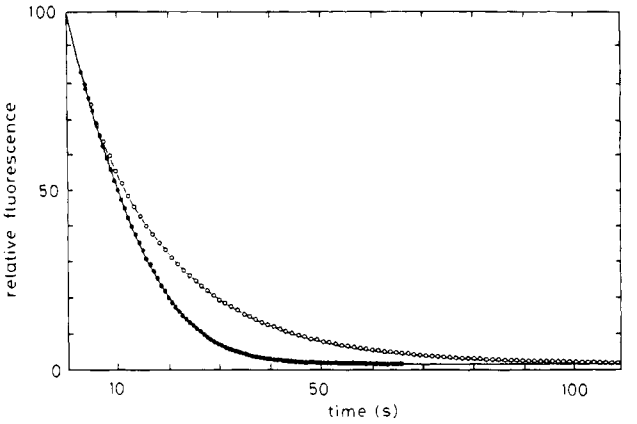

FIGURE 1: Progress curve analysis of the PRAI reaction. The conversion of 10 μM PRA by 7 nM xPRAI at 25 °C in buffer C is shown. The disappearance of PRA was followed by fluorescence excited at 310 nm and observed above 400 nm: (○) IGPS absent; (●) IGPS (540 nM) present in excess over xPRAI. The progress curves have been corrected for the small contribution to the fluorescence of PRT (and IGPS when added) present before the addition of xPRAI. In the absence of IGPS the fluorescence drops to approximately 4%, and in the presence of IGPS it drops to approximately 1% of its original value.

Table 1: Steady State Kinetic Constants of the PRAI Reaction: Comparison between Mono- and Bifunctional Variants

protein	$\bar{k}_{cat}$ (s^{-1})	K_M^{PRA} (μM)	$\bar{k}_{cat}/K_M^{PRA}$ ($\mu M^{-1} s^{-1}$)	K_M^{CdRP} (μM)	K_i^{rCdRP} (μM)
IGPS:PRAI	40	4.9	8.2	nd[a]	6.5
PRAI[ML256-452]	32	4.7	6.8	6.2	6.8
xPRAI	69	3.2	22	3.8	1.7

[a] nd: not determined.

which converts CdRP to IGP, leads to a further decrease in fluorescence excited at 310 nm, indicating that IGP exhibits approximately 1% of the fluorescence intensity of PRA (Figure 1). A reasonable fit to eq 1 of the progress curve measured in the absence of IGPS was not possible, but a fit to the integrated rate equation that explicitly takes product inhibition into account (eq 2; Duggleby & Morrison, 1977) gave an excellent result and yielded the product inhibition constant K_M^{CdRP}. The random nature and the small value of the residual fluctuations (not shown) testify to the good quality of the fit. The values of the steady state constants obtained for all three forms of PRAI are collected in Table 1. Control experiments showed that the accumulated IGP did not inhibit PRAI. Table 1 lists the values of K_M^{CdRP} for the two monomeric forms of PRAI. Because IGPS is fused to PRAI in IGPS:PRAI, K_M^{CdRP} of the PRAI domain cannot be determined in this case.

Previous work had shown that rCdRP independently binds to two sites on IGPS:PRAI (Bisswanger et al., 1979). The site of relatively high affinity for rCdRP was shown to be identical to the active site of IGPS by competitive inhibition studies. By inference, the site with relatively low affinity should be the active site of PRAI. We therefore decided to determine directly the mode and strength of inhibition of monofunctional PRAI by rCdRP.

Since rCdRP fluoresces when excited at 310 nm, and thus produces a high background signal, we turned from the analysis of progress curves to the analysis of initial velocities. rCdRP does not affect the catalytic rate constant (data not shown), meaning that it competes with PRA. Moreover, the

apparent K_M^{PRA} increases linearly with the concentration of inhibitor, as expected for competitive inhibition, yielding the values for K_i^{rCdRP} collected in Table 1. Again there is only a minor difference between the connected and excised PRAI domains, but the inhibition constant of xPRAI is significantly smaller.

Steady State Kinetics of the Reverse PRAI Reaction. The low fluorescence quantum yield of CdRP by comparison to PRA and the almost complete disappearance of the fluorescence during the conversion of PRA to CdRP already indicate that the thermodynamic equilibrium strongly favors CdRP (cf. Figure 1). However, PRA spontaneously and irreversibly hydrolyzes to anthranilate with a half-life of 3.5 min at pH 7.6 (Creighton, 1968). Thus, the unfavorable CdRP → PRA reaction is enforced by the favorable hydrolysis of PRA and can be followed by the appearance of the strong fluorescence of anthranilate.

The first-order rate constant, k_h, of the spontaneous hydrolysis of PRA was measured by first synthesizing PRA from PRPP and an excess of anthranilate in the presence of Mg^{2+} ions and PRT. The fluorescence of anthranilate reappeared after the limiting PRPP had been exhausted. The reappearance of fluorescence followed a single exponential for a rate constant (k_h) of 1.9×10^{-3} s^{-1} (data not shown), in close agreement with the half-life of PRA determined by Creighton (1968) under similar conditions.

Figure 2A shows the evolution of difference absorbance spectra after the addition of xPRAI to CdRP. Isosbestic points were discernible at 279 and 312 nm, indicating that only two components contribute to the absorbance spectra. Moreover, the difference spectra precisely fitted the difference spectrum, CdRP − anthranilate (Kirschner et al., 1987), whereas no detectable component of the difference spectrum CdRP − PRA was present. Thus, CdRP apparently is converted to anthranilate without accumulating PRA. This conclusion is buttressed by the diagnostic absorbance versus absorbance plots. The linear dependence of both A_{300} and A_{336} on A_{258} (data not shown) indicates that there is only one observable first-order process, namely, the overall conversion of CdRP to anthranilate. The difference absorbance at 258 nm decreased exponentially with $k_{obs} = 4.2 \times 10^{-5}$ s^{-1} (Figure 2B). The same value was determined with 0.2 μM PRAI[MS256-452], and the increase to 2.0 μM PRAI[ML256-452] had no effect. In the absence of PRAI, no significant disappearance of CdRP occurs (not shown). Thus, the decomposition of CdRP to anthranilate in the presence of PRAI is rate-limited by an uncatalyzed first-order process.

Single-Turnover Kinetics of the Forward PRAI Reaction. The PRAI reaction is well poised for rapid-mixing experiments under single-turnover conditions. By mixing a limiting concentration of PRA with an excess concentration of enzyme, most of the available PRA will be rapidly bound to the enzyme, followed by its conversion to product. Because both PRA and CdRP have the same anthranilate moiety as rCdRP (Bisswanger et al., 1979; Cohn et al., 1979), both the binding steps and the ensuing chemical reaction should be detectable by the perturbation in the fluorescence of either tryptophan (protein), PRA, or both. Moreover, since CdRP has negligible fluorescence, the overall chemical reaction (PRA → CdRP) should lead to a decrease in fluorescence.

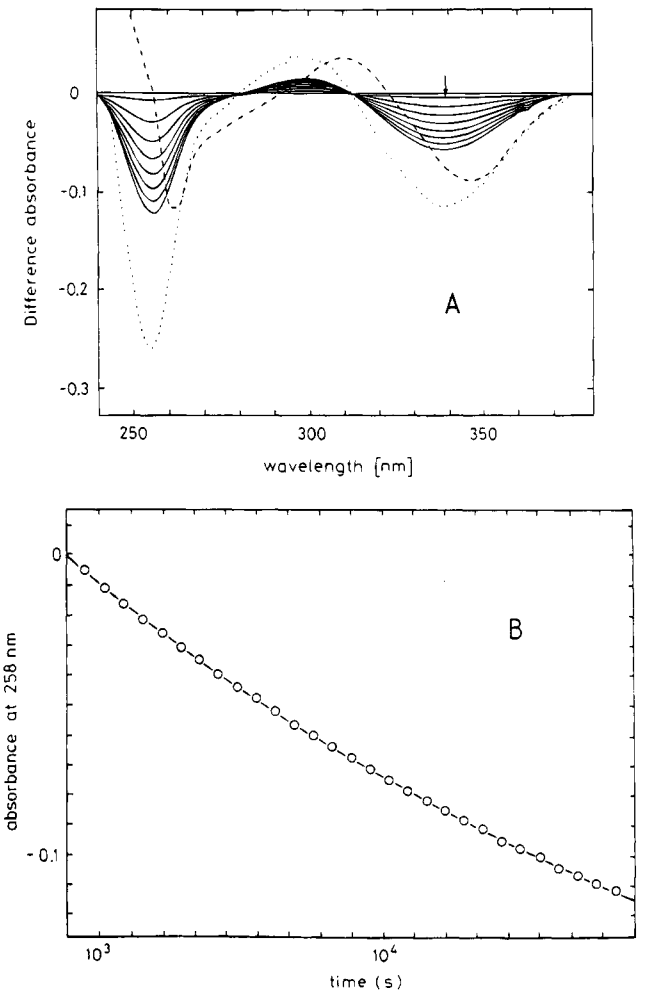

FIGURE 2: Catalysis of the hydrolysis of CdRP to anthranilate to PRAI. (A) Difference spectra of 75 μM CdRP in buffer C at 25 °C, after the addition of 0.2 μM xPRAI: (arrow) first recording after 10 min, subsequent recordings after intervals of 30 min; (dotted line) difference spectrum of 50 μM (CdRP − anthranilate); (dashed line) difference spectrum of 50 μM (CdRP − PRA). (B) Progress curve of decay of CdRP: (○) buffer C, 25 °C, 50 μM CdRP, and 1 μM xPRAI: (solid line) fit to a single exponential with $k_{obs} = 4.2 \times 10^{-5}$ s^{-1}. The same rate constant was determined with PRAI-[ML256-452] and concentrations of enzyme ranging from 0.2 to 2 μM.

We varied the concentrations under approximately first-order conditions by varying the enzyme concentration at a fixed ratio to that of PRA ($[PRAI]_0/[PRA]_0 = 10$). We used the monofunctional domain of the *E. coli* enzyme (PRAI-[ML256-452]) for these experiments, and the total enzyme concentration was varied between 2 and 25 μM. Rapid mixing of PRA with PRAI[ML256-452] results in a decrease in fluorescence for both PRA (F_{310}^{400}) and the enzyme (F_{280}^{340}). In contrast to the binding of rCdRP (Cohn et al., 1979), fluorescence energy transfer from excited tryptophan to bound PRA (F_{280}^{420}) gave no observable transients. Since the fluorescence of PRA was larger than that of the enzyme, the former was used for the analysis single turnovers of PRA.

Figure 3A,B shows the rapid and slow transients observed with PRAI[ML256-452]. The fluorescence decreased to insignificant levels in two phases according to

$$\Delta F_t = \Delta F_1^0 e^{-tk_{obs,1}} + \Delta F_2^0 e^{-tk_{obs,2}} \quad (3)$$

where ΔF_t is the deviation in fluorescence at time t from

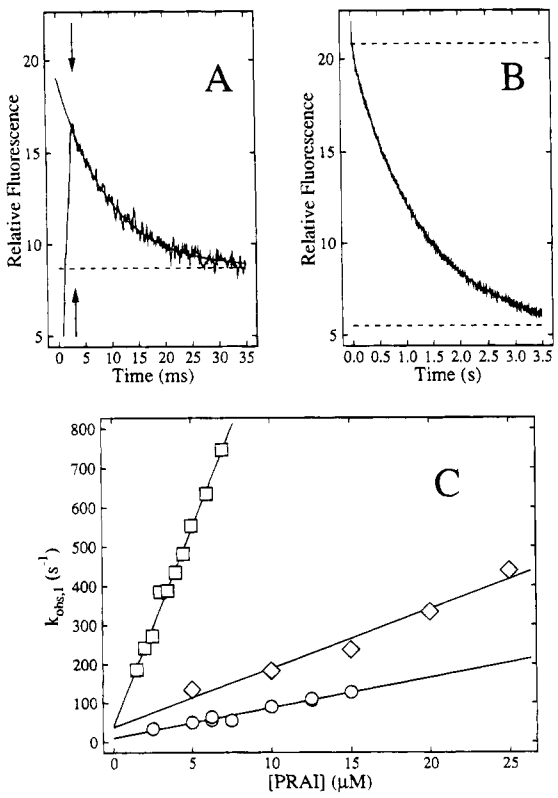

FIGURE 3: Single turnovers of PRA catalyzed by PRAI. Experiments were performed in buffer C at 25 °C. Values refer to initial concentrations after mixing. (A) Rapid phase (single transient) obtained by mixing PRAI[ML256-452] (12.5 μM) with PRA (1.25 μM). Arrows indicate the stop of flow; the solid line is a least-squares fit to a single exponential ($k_{obs,1}$ = 107 s^{-1}). (B) Slow phase of the experiment shown in (A). A slow phase of the same rate constant ($k_{obs,2}$ = 0.85 s^{-1}) was also observed in the case of xPRAI and IGPS:PRAI. (C) Evaluation of $k_{obs,1}$: (◇) IGPS:PRAI; (□) xPRAI; (○) PRAI[ML256-452]. Each point represents values of $k_{obs,1}$ averaged from 5−20 individual transients.

the final equilibrium value, ΔF_1^0 and ΔF_2^0 are the fluorescence amplitudes, and $k_{obs,1}$ and $k_{obs,2}$ are the observed rate constants of the rapid and slow processes, respectively.

Figure 3C shows that $k_{obs,1}$ increases linearly with the total concentration of excess enzyme, as expected for an elementary binding reaction (Bernasconi, 1976; Hiromi, 1978):

$$k_{obs,1} = k_D + k_R[PRAI]_0 \quad (4)$$

where $[PRAI]_0$ is the total concentration of excess enzyme, and k_D and k_R are the rate constants of dissociation and recombination, respectively. The values of k_D and k_R obtained from the intercepts and slopes of the straight lines in Figure 3C with the three forms of PRAI are collected in Table 2. Although the recombination rate constants k_R differ by more than 10-fold, the equilibrium constants $k_D/k_R = K_d^{PRA}$ differ only by a factor of 4.

In contrast to $k_{obs,1}$ the first-order rate constant $k_{obs,2}$ (~1 s^{-1}) was independent of the concentration and source of enzyme used. Its amplitude linearly depended on the concentrations of substrate and enzyme used at a molar ratio of 1:10 and amounted to 60% of the total fluorescence [$\Delta F_2^0/(\Delta F_1^0 + \Delta F_2^0) = 0.6$; data not shown].

Spontaneous Isomerization of the Primary Product of PRAI. It was puzzling that no first-order process with a rate constant higher than or equal to $\vec{k}_{cat}$ (32 s^{-1} in the case of PRAI[ML256-452], cf. Table 1) was observed. The slow phase of the single turnover of PRA obviously represents the rate-limiting step and should be due to either the chemical conversion of the PRAI−PRA to the PRAI−CdRP complex, the release of CdRP from PRAI−CdRP, or a combination of both. However, the value of $k_{obs,2}$ (~1 s^{-1}) is much too small to account for any step in the catalytic conversion of PRAI to CdRP, including the release of the product, CdRP; due to the measured value of $\vec{k}_{cat}$ (Table 1), no elementary rate constant can be smaller than about 30 s^{-1}.

We considered two alternative explanations for the slow phase. Model 1 assumes that PRA consists of an equilibrium mixture between two equally fluorescent isomers, αPRA and βPRA:

$$PRAI + \alpha PRA \overset{slow}{\longleftrightarrow} PRAI + \beta PRA \overset{fast}{\longleftrightarrow} PRAI + CdRP^\circ \quad (5)$$

where βPRA is a reaction competent species and αPRA is a reaction incompetent species. Although enzymically generated PRA is probably 100% β-anomer (Hommel et al., 1989), phosphoribosylamine is known to isomerize slowly and spontaneously to a mixture of the α- and β-anomers (Schendel et al., 1988). In a single-turnover experiment with PRAI, the limiting competent substrate βPRA would be consumed in the rapid reaction, followed by the slow, spontaneous, first-order conversion of αPRA to βPRA, which is independent of the concentration of enzyme.

Model 2 assumes that the primary product released from PRAI is a fluorescent isomer of CdRP (CdRP*) that spontaneously decays to a stable, nonfluorescent isomer (CdRP°). Thus, CdRP will be a mixture of CdRP* and CdRP°, which favors CdRP° at equilibrium:

$$PRAI + PRA \overset{fast}{\longleftrightarrow} PRAI + CdRP^* \overset{slow}{\longleftrightarrow} PRAI + CdRP^\circ \quad (6)$$

In a single-turnover experiment with PRAI, the limiting substrate PRA would be converted to CdRP* in the rapid reaction, followed by the slow, spontaneous conversion of CdRP* to CdRP°.

Assuming that the competent substrate of PRAI is the β-anomer, we considered the possibility of rapidly generating anomerically pure βPRA from PRPP and anthranilate in situ, so that its postulated spontaneous isomerization to αPRA would not have had time to proceed before it was consumed by the PRAI reaction. However, the half-life period of formation of PRA, which is limited by k_{cat} of PRT [$t_{1/2} = \ln(2/k_{cat}) = 0.69/2.9 \sim 0.24$ s; Hommel et al., 1989], is too long. Further, we reasoned that, with the presence of two equally fluorescent isomers of PRA in model 1 (eq 5), instant inactivation of PRAI just after the initial phase (say, after 1 s; cf. Figures 3A and 5B) should prevent a further slow decrease in fluorescence. In contrast, with the slow conversion of a fluorescent to a nonfluorescent isomer of the primary product, as postulated by model 2 (eq 6), instant inactivation after the initial step should not prevent a further slow decrease in fluorescence.

In order to inactivate PRAI rapidly, a solution containing 4 M GuCl was mixed in a ratio of 1/6 with the solution containing PRAI, giving a final concentration of 0.67 M GuCl. As a control, the rate of inactivation of PRAI by 0.67 M GuCl was measured by first mixing enzymatically

Table 2: Rate and Equilibrium Constants and Ligand Binding to Three Forms of PRAI: Results of Transient Kinetics

	PRA				CdRP			rCdRP				
protein	k_D (s^{-1})	k_R (μM^{-1} s^{-1})	k_D/k_R (μM)	$k_{obs,2}$ (s^{-1})	k_D (s^{-1})	k_R (μM^{-1} s^{-1})	k_D/k_R (μM)	k_D (s^{-1})	k_R (μM^{-1} s^{-1})	k_D/k_R (μM)	K_d^{rCdRP} (μM)	K_i^{rCdRP} [a] (μM)
IGPS:PRAI	34	15	2.2	nd[b]	nd	nd	nd	140[c]	14[c]	10	12.5[d]	6.5
PRAI[ML256-452]	8.9	8	1.1	0.87	190	32	5.9	280	23	12	7.9[e]	6.8
xPRAI	47	100	0.47	1.1	161	68	2.4	112	77	1.5	1.8	1.7

[a] From Table 1. [b] nd: not determined. [c] Cohn et al. (1979). [d] Bisswanger et al. (1979). [e] cf. Figure 6B.

prepared PRA in a three-syringe, multiple-mixing apparatus with GuCl to 0.67 M and, after a delay period of 1 s, adding native PRAI at a 10-fold molar excess over PRA. Since no fluorescence decrease was observable (data not shown), PRAI must have been inactivated within the mixing time.

Inactivation of PRAI after the rapid phase of the decay of PRA showed that the slow process continued nevertheless (Figure 4A). Moreover, the total fluorescence change was the same as that observed in a control experiment without the inactivation of PRAI[ML256-452], i.e., where the GuCl solution was replaced by buffer. The somewhat smaller rate constant of the slow process measured in the presence of GuCl (0.49 s^{-1}), compared with the value obtained in the absence of denaturant (0.95 s^{-1}), may be due to the different ionic compositions of the solvents.

The assumption of equal fluorescence quantum yields for the two putative isomers αPRA and βPRA of the substrate (eq 5) may be incorrect. We therefore designed the following coupled spectrophotometric single-turnover experiment as an independent check. In the presence of excess monofunctional IGPS[1-259], either CdRP*, CdRP°, or both would be converted to IGP + CO_2. This reaction can be monitored specifically via the increasing fluorescence of IGP (Hankins et al., 1975):

$$\text{CdRP°,CdRP*} \xrightarrow{\text{IGPS}} \text{IGP} + CO_2 \qquad (7)$$

Model 1 (eq 5) predicts biphasic production of CdRP, which, in the presence of excess IGPS[1-259], must lead to biphasic production of IGP. In contrast, model 2 (eq 6) predicts monophasic production of CdRP°. It is not known whether CdRP°, CdRP*, or both are competent substrates for IGPS-[1-259].

The experiment showed that the fluorescence of IGP increased with a single-exponential phase without an initial lag (Figure 4B, trace 1). The rate constant (0.96 s^{-1}) was the same as that of the slow phase of the PRAI reaction proceeding in the absence of IGPS[1-259] (Figure 3B). As a control, we measured the single turnover of the same concentration of IGPS[1-259] after rapidly mixing it with a concentration of CdRP equivalent to the concentration of PRA in the previous experiment (Figure 4B, trace 2). Again, only a single-exponential increase in fluorescence was observed, but the rate constant was 3-fold larger, corresponding to the known value of k_{cat} of IGPS[1-259] (Eberhard et al., 1995). These results confirm that the stable isomer of the product (CdRP°) is the competent substrate of IGPS-[1-259] and that the slow process observed in the coupled assay (trace 1) is not rate-limited by the response of IGPS-[1-259] (trace 2).

These data are consistent with model 2 and rule out model 1. Because IGP is produced with the same rate constant as the slow phase of the PRAI reaction, the primary product

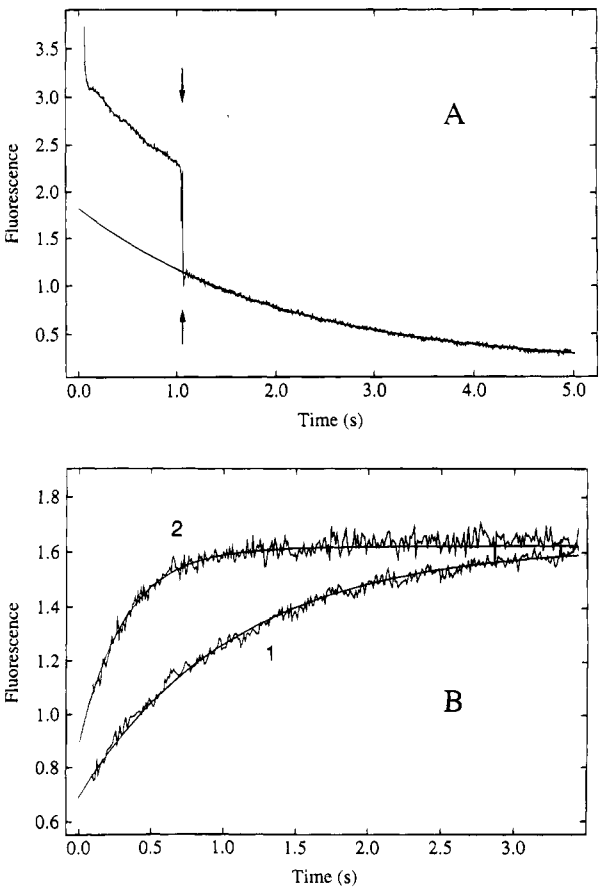

FIGURE 4: Slow phase of the progress curve observed after the mixing of PRA with PRAI due to tautomerization of the initially formed product (single-turnover conditions). Values refer to initial concentrations after mixing. (A) Fluorescence of PRA excited at 310 nm and observed above 395 nm. The PRAI reaction was initiated by rapidly mixing PRA (1.5 μM) with PRAI[ML256-452] (15 μM). After 1 s (arrows), PRAI in the reaction mixture was inactivated instantaneously by rapid mixing with 4 M GuCl to PRA (1.0 μM), PRAI (10 μM), and GuCl (0.67 M). The solid line is a least-squares fit to a single exponential with $k_{obs,2}$ = 0.49 s^{-1}. The first, rapid phase ($k_{obs,1}$; cf. Figure 3) is not visible here. (B) Use of IGPS to convert nascent product (CdRP) to IGP; fluorescence of IGP excited at 280 nm and observed above 345 nm. (1) The PRAI reaction was initiated by rapidly mixing PRA (2.0 μM) with PRAI[ML256-452] and IGPS[1-259] (both at 18 μM). The solid line is a least-squares fit to a single exponential with k_{obs} = 0.96 s^{-1}. (2) The IGPS reaction was initiated by rapidly mixing enzymatically prepared, equilibrated CdRP (2.0 μM) with IGPS-[1-259] (18 μM). The solid line is a least-squares fit to a single exponential with k_{obs} = 3.27 s^{-1}.

CdRP* is not competent for the IGPS reaction. Moreover, the conversion of CdRP* to CdRP° is not catalyzed by either PRT, PRAI, or IGPS. Since the slow phase in the single-turnover experiment corresponding to the spontaneous isomerization of CdRP* accounts for 60% of the total fluorescence signal, the mixture of PRA and CdRP* present

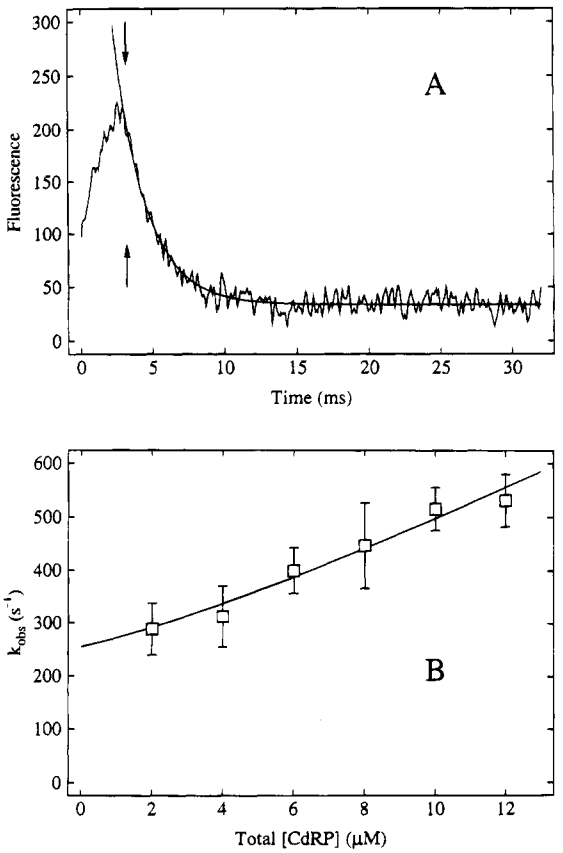

FIGURE 5: Kinetics of CdRP binding to PRAI[ML256-452]. Values refer to initial concentrations after mixing. (A) Single stopped-flow transient observed after mixing CdRP (2 μM) with PRAI-[ML256-452] (6 μM). The arrows indicate where the flow stopped. The solid line is a least-squares fits to a single exponential (k_{obs} = 452 s^{-1}). (B) Dependence of k_{obs} on CdRP concentration. Each point represents an average of k_{obs} from 10−15 individual transients; the vertical lines represent the standard deviation of the average. The solid line is a fit of the data to eq 3 in Eberhard et al. (1995), with the rate constants as collected in Table 2.

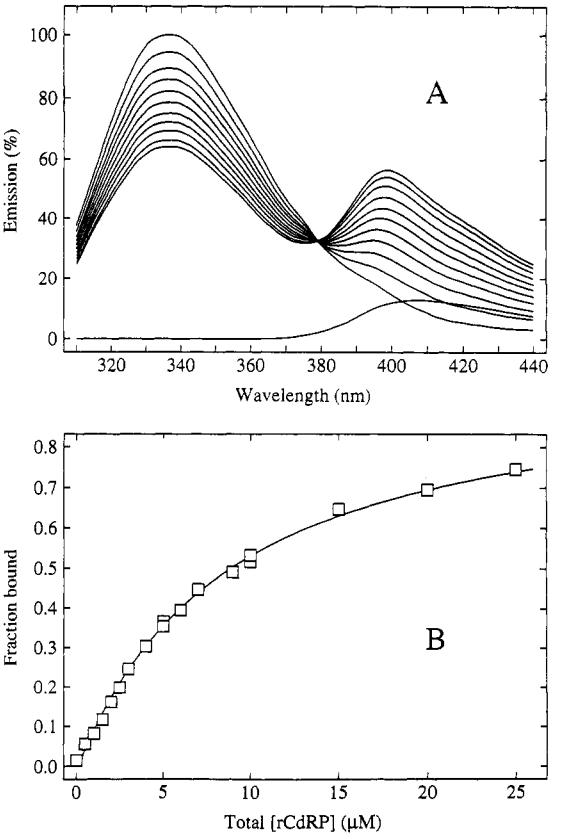

FIGURE 6: Fluorescence titration of PRAI[ML256-452] with rCdRP. (A) Spectral changes. PRAI[ML256-452] (2.1 μM), in buffer C at 25 °C, was titrated with rCdRP in increments of 0.5 μM. Fluorescence excited at 280 nm increased at 338 nm and decreased at 400 nm upon the addition of rCdRP. The bottom curve represents the emission spectrum of 10 μM rCdRP in the absence of PRAI-[ML256-452]. The spectra were corrected for dilution by ligand solution (0.5% per step). (B) Determination of the thermodynamic dissociation constants; evaluation of fluorescence quenching at 350 nm, where rCdRP does not contribute to the signal. The least-squares fit [eq 1 in Eberhard et al. (1995)] yields n = 0.95 and K_d^{rCdRP} = 7.8 μM.

before the onset of isomerization exhibit considerable fluorescence. If we assume that a substantial fraction of PRA is converted to CdRP* during the first rapid phase (cf. Discussion), CdRP* may exhibit up to 60% of the fluorescence quantum yield of PRA. The fluorescence signal drops during the slow phase of the reaction to very low values, indicating that CdRP, henceforth denoting the equilibrium mixture of CdRP* and CdRP°, favors CdRP°, which exhibits virtually no fluorescence. This conclusion is supported by the residual fluorescence observed after the conversion of PRA to CdRP by PRAI (Figure 1).

Transient Kinetics of CdRP Binding to PRAI. The rate of binding of CdRP was measured to determine the thermodynamic dissociation constant of the PRAI−CdRP complex (K_d^{CdRP}) for comparison to the K_M^{CdRP} value from product inhibition (cf. Table 1). Because the fluorescence of CdRP is negligible by comparison to that of PRA, we used the quenching of tryptophan fluorescence (F_{280}^{340}) as a signal to follow the binding reactions. In this case, the total concentration of PRAI was kept constant at 6 μM, and the concentration of CdRP was varied between 2 and 12 μM.

Figure 5A shows, again with PRAI[ML256-452] as an example, that the binding of CdRP is observed as a rapid, single-exponential process ($\Delta F_t = \Delta F^0 e^{-tk_{obs}}$). Figure 5B presents the plot of k_{obs} versus the concentration of total CdRP. The increase indicates qualitatively that the transient reflects an elementary binding step. The data were fitted to the exact expression relating k_{obs} to the total concentrations of both CdRP and active sites (Eberhard et al., 1995), and the computed values of k_D and k_R are collected (together with the rate constants pertaining to xPRAI) in Table 2. As expected from the overall equilibrium favoring CdRP over PRA, and the small value of k_{obs} for the conversion of CdRP to anthranilate (4.2×10^{-5} s^{-1}, see earlier), no further process related to any chemical interconversions was observed in Figure 5A. Moreover, the values of the thermodynamic dissociation constants $K_d^{CdRP} = k_D/k_R$ agree reasonably well with the values of K_M^{CdRP} determined from product inhibition (cf. Table 1).

Transient Kinetics of rCdRP Binding to PRAI. The equilibria and rates of binding of the competitive inhibitor rCdRP to monomeric PRAI[ML256-452] are of particular interest, because previous measurements had been performed with the bifunctional wild-type IGPS:PRAI (Bisswanger et al., 1979; Cohn et al., 1979). In that case, the binding to active sites of both PRAI and IGPS led to an overlap of the individual contributions to the overall progress curves.

By using data obtained with PRAI[ML256-452] as an example, Figure 6A shows how tryptophan fluorescence at

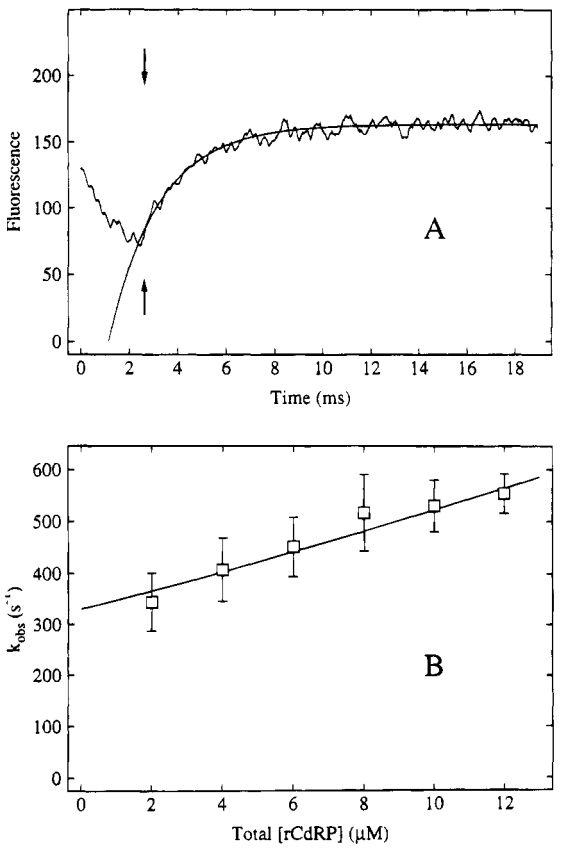

FIGURE 7: Kinetics of rCdRP binding to PRAI[ML256-452]. Stopped-flow measurements were performed in buffer C at 25 °C. Values refer to initial conditions after mixing. (A) Typical stopped-flow transient observed after the mixing of PRAI[ML256-452] (2 μM) with rCdRP (8 μM). Fluorescence was excited at 280 nm and observed with a bandpass filter (330−380 nm). The arrows indicate where the flow stopped. The solid line depicts the exponential calculated by least-squares methods (k_{obs} = 478 s^{-1}). (B) Determination of the association and dissociation rate constants. The solid line is the best fit of k_{obs} to eq 3 in Eberhard et al. (1995), with k_D = 280 s^{-1} and $k_R = 2.3 \times 10^7$ M^{-1} s^{-1} (cf. Table 2). Each point represents the average of k_{obs} from approximately 10 stopped-flow transients. The vertical lines indicate the standard deviations of the average.

335 nm is quenched by the inhibitor rCdRp and that fluorescence energy transfer from tryptophan to rCdRP increases (F_{280}^{400}) when a constant concentration of enzyme is titrated with increasing concentrations of the inhibitor. In contrast to IGPS:PRAI (Bisswanger et al., 1979) or IGPS-[1-259] (Eberhard et al., 1995), the intrinsic fluorescence of CdRP (F_{320}^{420}) is quenched only to a minor degree upon the addition of excess PRAI[ML256-452] (data not shown). A nonlinear least-squares fit of the data to the elementary binding reaction (cf. Eberhard et al., 1995) is shown in Figure 6B and yields the values of the number of binding sites per monomer (n = 0.95) and K_d^{rCdRP} (Table 2). Comparison to the entries in Table 1 shows reasonable agreement of these values with the independently determined competitive inhibition constants K_i^{rCdRP}.

The kinetics of rCdRP binding was followed either by protein fluorescence quenching (F_{280}^{340}) or by fluorescence energy transfer (F_{280}^{420}). Only a single transient was observed after the rapid mixing of PRAI[ML256-452] with an excess of rCdRP (Figure 7A). A fit of k_{obs} to the exact expression relating k_{obs} to the concentration of rCdRP gave the values of both k_D and k_R, the dissociation and recombination rate constants, respectively. Compared to the values obtained with PRAI[ML256-452] (Table 2), the values obtained with xPRAI (transients not shown) are at most 3-fold different. Again, the ratio k_D/k_R agrees reasonably well with the equilibrium constants K_d^{rCdRP} and K_i^{rCdRP} determined independently.

Scheme 2

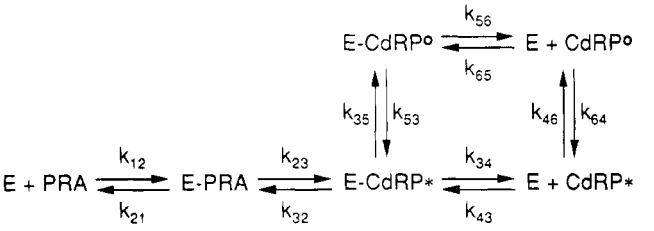

DISCUSSION

The use of purified enzymes to prepare PRA and CdRP has prepared the way for elucidating the formal catalytic mechanism of PRAI. Both steady state and transient kinetic results show that (i) the metabolic reaction is reversible, but strongly favors a stable, nonfluorescent isomer of CdRP; (ii) the first product is a partially fluorescent, metastable isomer of CdRP, termed CdRP*; (iii) the binding of PRA to the active site and its conversion to bound CdRP* cannot be separated experimentally into two elementary steps; (iv) CdRP* isomerizes slowly and spontaneously to CdRP°, which is also the true substrate of the IGPS reaction; and (v) the artificially excised PRAI domain is almost indistinguishable from its naturally fused state in the bifunctional enzyme from *E. coli*. It is somewhat more sluggish than the naturally monofunctional xPRAI from yeast.

Scheme 2 presents a formal mechanism that is consistent with the results of the present study. PRAI catalyzes the interconversion of PRA and CdRP*, which is followed by the spontaneous conversion of CdRP* to CdRP°. Whereas the thermodynamic equilibrium between CdRP* and PRA could be rather balanced, the overall reaction is driven by the spontaneous isomerization that strongly favors CdRP°. In the following, we designate the equilibrium mixture of CdRP* and CdRP° as CdRP.

The reverse reaction (CdRP → PRA) requires the presence of enzyme and can only be observed by coupling it to the irreversible spontaneous hydrolysis of PRA to anthranilate and, presumably, ribose 5-phosphate (eq 8). Since the enzymatic interconversion of PRA to CdRP is much faster than the spontaneous hydrolysis of PRA, the concentrations of CdRP and PRA are close to their equilibrium values during the reaction:

$$\text{CdRP} \leftrightarrow \text{PRA} \xrightarrow{k_h} \text{anthranilate} + \text{ribose 5-phosphate} \quad (8)$$

Thus, the rate of enzyme-catalyzed hydrolysis of CdRP to anthranilate is given by

$$-\text{d[CdRP]}/\text{d}t = k_h[\text{PRA}] = k_h[\text{CdRP}]/K' = k_{obs}[\text{CdRP}] \quad (9)$$

The value of the overall equilibrium constant, K' = [CdRP]/[PRA], is calculable from the values of k_h and k_{obs} measured independently ($K' = k_h/k_{obs} = 1.9 \times 10^{-3}/4.2 \times 10^{-5} = 45$).

During the turnover of PRA, the primary product CdRP* is formed in a single second-order process, that is, the chemical conversion was not observable as a separate process. Thus, the values of k_D and k_R of PRA (Table 2) are not identical with k_{21} and k_{12}, respectively, but also depend on the chemical step (k_{23} amd k_{32}, Scheme 2). Due to the equilibrium between CdRP* and CdRP°, which favors CdRP°, the amplitude of CdRP* binding is too small to be observed; only the overall binding of CdRP can be determined. k_D and k_R of CdRP binding correspond to k_{56} and k_{65}, respectively, but also depend on k_{34} and k_{43} to a minor extent (Scheme 2). It is interesting to note that the rate constants of rCdRP binding to PRAI are close to those of CdRP, despite the structural differences between the compounds.

The rate constant of the slow phase of the single-turnover transients was independent of the total excess enzyme concentration ($k_{obs,2} = 1\ s^{-1}$; cf. Figure 3B). The simplest explanation is that PRAI does not catalyze the conversion of CdRP* to CdRP°. Thus, the rate constants of the interconversion of enzyme-bound CdRP* and CdRP° (k_{35} and k_{53} in Scheme 2) are either smaller than or equal to those of the free products (k_{46} and k_{64} in Scheme 2). Due to the slow phase of the single-turnover transients, k_{46} is approximately 1 s^{-1}, and k_{64} must be significantly smaller than 1 s^{-1} since CdRP° predominates over CdRP* at equilibrium. Inspection of the equations relating the steady state constants to the individual rate constants of Scheme 2 (cf. Appendix) reveals that the values of k_{35} and k_{53} do not markedly affect the catalytic constants and Michaelis constants of both the forward and reverse reactions as long as $k_{35} \leq k_{46}$, $k_{53} \leq k_{64}$, and the requirement of the thermodynamic cycle ($k_{34}k_{46}k_{65}k_{53} = k_{43}k_{35}k_{56}k_{64}$) are valid. Therefore, the noncatalyzed conversion of CdRP* to CdRP° is consistent with the measured steady state parameters and the overall equilibrium constant. The turnover numbers (k_{cat}) of both forward and reverse reactions are not limited by the rate constant of isomerization between CdRP* and CdRP° (cf. Scheme 2). In the forward reaction, only k_{23} and k_{34} contribute to the release of free enzyme for the next catalytic cycle. In the reverse reaction, only k_{21} and k_{32} contribute to the release of free enzyme, whereas E−CdRP* and E−CdRP° are at equilibrium.

It is remarkable that the biosynthesis of tryptophan, i.e., the conversion of PRA to IGP, involves an apparently uncatalyzed interconversion of two isomers of CdRP. Due to their fluorescence properties (cf. Results), it is tempting to assume that CdRP* is the enolamine and CdRP° the ketoamine tautomer (cf. Scheme 1). If the concentrations of the intermediate metabolites of tryptophan biosynthesis and that of the participating enzymes were in the micromolar range (i.e., equivalent to the K_M values of the respective enzymes), then the rate of the uncatalyzed step would be on the order of 1 $\mu M\ s^{-1}$ and that of the enzymatic steps 10−100 $\mu M\ s^{-1}$ (assuming k_{cat} values to range between 10 and 100 s^{-1}); the overall flow would be limited by the spontaneous tautomerization of CdRP* to CdRP°. Even if the "electrostatic valley" (Stroud, 1994) could arise by evolution to connect the active sites of PRAI and IGPS, it would be useless because the limiting isomerization is slow (1 s^{-1}; cf. Figure 5B). A different advantage gained by the fusion of IGPS and PRAI must have led to the selection of the bifunctional enzyme in *E. coli* (Eberhard et al., 1995). However, it cannot be excluded that *E. coli* contains an as yet unidentified enzyme catalyzing the preceding conversion. In mammalian cells, dopachrome tautomerase (Aroca et al., 1990), *N*-acetyldopaminequinone tautomerase (Sugumaran et al., 1989), and oxaloacetate ketoenol tautomerase (Belikova et al., 1988), which catalyze chemically analogous reactions, have been identified and characterized. In *Pseudomonas putida*, a 4-oxalocrotonate tautomerase has been described (Harayama & Rekik, 1990). Although all enzymes of the tryptophan operon of *E. coli* have been analyzed and characterized, one of them might carry the putative CdRP tautomerase as an additional activity, or a CdRP tautomerase may be encoded by a gene unlinked to the tryptophan operon. Both possibilities seem to be quite unlikely. As demonstrated by single-turnover experiments, neither PRT, PRAI, nor IGPS catalyzes the interconversion of the two isomers of CdRP.

APPENDIX

Calculation of the Steady State Constants of Scheme 2. Three assumptions were made: E, E−PRA, E−CdRP*, and E−CdRP° are in steady state; the reaction CdRP* ↔ CdRP° is in equilibrium under steady state conditions; and the concentrations of substrate, [PRA], and products, [CdRP*] and [CdRP°], are much larger than those of the components present at the steady state level (E, E−PRA, E−CdRP*, and E−CdRP°) and therefore are constant throughout the measurement of initial velocities. Note that CdRP* represents the fluorescent isomer and CdRP° the nonfluorescent isomer of CdRP. K_M^{CdRP*} and $K_M^{CdRP°}$ are the Michaelis constants and k_{cat}^{CdRP*} and $k_{cat}^{CdRP°}$ are the catalytic constants due to CdRP* and CdRP°, respectively. The catalytic constants are not identical, as will be shown here. k_{cat} and K_M^{CdRP} are the overall steady state constants of the reverse reaction (CdRP → PRA), and k_{cat}^{PRA} and K_M^{PRA} are those of the forward reaction (PRA → CdRP). The indices of the rate constants are defined according to the numbering of the corresponding states (Bernasconi, 1976). Scheme 2 defines the following rate equations:

$$d[E]/dt = -k_{12}[PRA][E] + k_{21}[E-PRA] + k_{34}[E-CdRP*] - k_{43}[CdRP*][E] + k_{56}[E-CdRP°] - k_{65}[CdRP°][E]$$

$$d[E-PRA]/dt = k_{12}[PRA][E] - k_{21}[E-PRA] - k_{23}[E-PRA] + k_{32}[E-CdRP*]$$

$$d[E-CdRP*]/dt = k_{23}[E-PRA] - k_{32}[E-CdRP*] - k_{34}[E-CdRP*] + k_{43}[CdRP*][E] - k_{35}[E-CdRP*] + k_{53}[E-CdRP°]$$

$$d[E-CdRP°]/dt = k_{35}[E-CdRP*] - k_{53}[E-CdRP°] - k_{56}[E-CdRP°] + k_{65}[CdRP°][E]$$

The initial velocity, V_i, is given by

$$V_i = d[CdRP°]/dt + d[CdRP*]/dt = -d[PRA]/dt = k_{12}[PRA][E] - k_{21}[E-PRA] = k_{34}[E-CdRP*] - k_{43}[CdRP*][E] + k_{56}[E-CdRP°] - k_{65}[CdRP°][E]$$

By virtue of the steady state assumption, d[E]/dt = d[E−PRA]/dt = d[E−CdRP*]/dt = d[E−CdRP°]/dt = 0. The initial velocity (V_i) of the reaction may be formally dissected into three contributions, namely, those of PRA, CdRP*, and CdRP°:

$$V_i = \frac{k_{cat}^{PRA}[E][PRA]}{[PRA] + K_M^{PRA}(1 + [CdRP^*]/K_M^{CdRP^*} + [CdRP^\circ]/K_M^{CdRP^\circ})} - \frac{k_{cat}^{CdRP^*}[E][CdRP^*]}{[CdRP^*] + K_M^{CdRP^*}(1 + [PRA]/K_M^{PRA} + [CdRP^\circ]/K_M^{CdRP^\circ})} - \frac{k_{cat}^{CdRP^\circ}[E][CdRP^\circ]}{[CdRP^\circ] + K_M^{CdRP^\circ}(1 + [PRA]/K_M^{PRA} + [CdRP^*]/K_M^{CdRP^*})}$$

The contribution of CdRP° and CdRP* to the forward reaction (the first term of the preceding equation) is identical to that of a competitive inhibitor. Therefore, the Michaelis constants of the reverse reaction ($K_M^{CdRP^*}$, $K_M^{CdRP^\circ}$) are identical to the product inhibition constant of the forward reaction. Similarly, the Michaelis constant of the forward reaction (K_M^{PRA}) is identical to the substrate inhibition constant of the reverse reaction.

The steady state constants of the preceding equation can be calculated as follows:

$$k_{cat}^{PRA} = k_{23}(k_{34}k_{53} + k_{34}k_{56} + k_{35}k_{56})/B$$

$$k_{cat}^{CdRP^*} = k_{21}(k_{32}k_{53} + k_{32}k_{56})/C$$

$$k_{cat}^{CdRP^\circ} = k_{21}k_{32}k_{53}/D$$

$$K_M^{PRA} = A/(k_{12}B)$$

$$K_M^{CdRP^*} = A/(k_{43}C)$$

$$K_M^{CdRP^\circ} = A/(k_{56}D)$$

where

$$A = (k_{21} + k_{23})(k_{34}k_{53} + k_{34}k_{56} + k_{35}k_{56}) + k_{21}k_{32}(k_{53} + k_{56})$$

$$B = (k_{53} + k_{56})(k_{23} + k_{32} + k_{34}) + k_{35}(k_{23} + k_{56})$$

$$C = (k_{21} + k_{23})(k_{35} + k_{53} + k_{56}) + k_{32}(k_{53} + k_{56})$$

$$D = (k_{21} + k_{23})(k_{34} + k_{35} + k_{53}) + k_{32}(k_{21} + k_{53})$$

This formalism treats CdRP° and CdRP* as if they were independent of each other ($k_{46} = k_{64} = 0$ in Scheme 2). In the present case, however, CdRP* and CdRP° are in equilibrium, and therefore, the ratio of their concentration is constant: i.e., [CdRP*]/[CdRP°] = k_{64}/k_{46}. Moreover, it is impossible to determine the steady state constants due to CdRP* and CdRP° separately; the only measurable parameters of the reverse reaction are the overall constants $\vec{k}_{cat}$ and K_M^{CdRP}. Therefore, it is reasonable to rewrite the preceding equations in order to express V_i in terms of the overall steady state constants:

$$\vec{k}_{cat} = k_{23}(k_{34}k_{53} + k_{34}k_{56} + k_{35}k_{56})/B$$

$$\vec{k}_{cat} = k_{21}k_{32}k_{53}(k_{34}k_{53} + k_{34}k_{56} + k_{35}k_{56})/(k_{34}k_{53}C + k_{35}k_{56}D)$$

$$K_M^{PRA} = A/(k_{12}B)$$

$$K_M^{CdRP} = A(k_{35}k_{43}k_{56} + k_{34}k_{53}k_{65})/(k_{43}k_{65}(k_{34}k_{53}C + k_{35}k_{56}D))$$

A, B, C, and D are defined earlier. Since E−CdRP*, E−CdRP°, CdRP*, and CdRP° form a thermodynamic cycle, [CdRP*]/[CdRP°] = $k_{64}/k_{46} = k_{34}k_{53}k_{65}/k_{43}k_{35}k_{56}$. If k_{34}, k_{53}, k_{65}, k_{43}, k_{35}, and k_{56} are adjusted so as to satisfy this equation, then d[CdRP°]/dt + d[CdRP*]/dt = −d[PRA]/dt.

It is instructive to examine the relationships between $k_{cat}^{CdRP^*}$, $k_{cat}^{CdRP^\circ}$, $\vec{k}_{cat}$, $K_M^{CdRP^*}$, $K_M^{CdRP^\circ}$, and K_M^{CdRP}:

$$\vec{k}_{cat} = \frac{[(k_{64}/k_{46})\,(k_{cat}^{CdRP^*}/K_M^{CdRP^*})] + (k_{cat}^{CdRP^\circ}/K_M^{CdRP^\circ})}{[(k_{64}/k_{46})\,(1/K_M^{CdRP^*})] + (1/K_M^{CdRP^\circ})}$$

$$K_M^{CdRP} = \frac{k_{64}/k_{46} + 1}{[(k_{64}/k_{46})\,(1/K_M^{CdRP^*})] + (1/K_M^{CdRP^\circ})}$$

If k_{64} is zero, then $\vec{k}_{cat}$ equals $k_{cat}^{CdRP^\circ}$. Conversely, if k_{46} decreases to zero, then $\vec{k}_{cat}$ approaches $k_{cat}^{CdRP^*}$. The steady state concentrations of E, E−PRA, E−CdRP*, and E−CdRP° may be expressed using the following equations:

$$[E] = [E]_0 a/(a + b + c + d)$$

$$[E{-}PRA] = [E]_0 b/(a + b + c + d)$$

$$[E{-}CdRP^*] = [E]_0 c/(a + b + c + d)$$

$$[E{-}CdRP^\circ] = [E]_0 d/(a + b + c + d)$$

with

$$a = (k_{21} + k_{23})(k_{34}k_{53} + k_{34}k_{56} + k_{35}k_{56}) + k_{21}k_{32}(k_{53} + k_{56})$$

$$b = [PRA]k_{12}((k_{32} + k_{34})(k_{53} + k_{56}) + k_{35}k_{56}) + [CdRP^*]k_{43}k_{32}(k_{53} + k_{56}) + [CdRP^\circ]k_{65}k_{32}k_{53}$$

$$c = [PRA]k_{12}k_{23}(k_{53} + k_{56}) + [CdRP^*]k_{43}(k_{21} + k_{23})(k_{53} + k_{56}) + [CdRP^\circ]k_{65}k_{53}(k_{21} + k_{23})$$

$$d = [PRA]k_{12}k_{23}k_{35} + [CdRP^*]k_{43}k_{35}(k_{21} + k_{23}) + [CdRP^\circ]k_{65}((k_{21} + k_{23})(k_{34} + k_{35}) + k_{21}k_{32})$$

Assuming k_{12} = 40 μM^{-1} s^{-1}, k_{21} = 200 s^{-1}, k_{23} = 50 s^{-1}, k_{32} = 20 s^{-1}, $k_{43} = k_{65}$ = 32 μM^{-1} s^{-1}, $k_{34} = k_{56}$ = 190 s^{-1}, $k_{35} = k_{46}$ = 0.9 s^{-1}, and $k_{53} = k_{64}$ = 0.06 s^{-1}, the following steady state constants result:

constant	unit	PRA	CdRP	CdRP*	CdRP°
k_{cat}	s^{-1}	36.552	0.9229	14.750	0.004638
K_M	μM	4.9519	5.9389	5.9605	5.9375
k_{cat}/K_M	μM^{-1} s^{-1}	7.3813	0.1554	2.4746	0.0007812

Here, k_{46}/k_{64} is assumed to be 15. Since the Michaelis constants of both isomers of CdRP are very similar, $k_{cat}^{CdRP^*}$ is close to $\vec{k}_{cat}k_{46}/k_{64}$, i.e., about 13.8 s^{-1}, and $k_{cat}^{CdRP^*}/K_M^{CdRP^*}$

is roughly a one-third of k_{cat}^{PRA}/K_M^{PRA}. Consequently, in a single-turnover experiment, PRAI rapidly establishes a 1/3 mixture of PRA and CdRP*, followed by an uncatalyzed decay of CdRP* to CdRP°.

REFERENCES

Aroca, P., Solano, F., Garcia-Borron, J. C., & Lozano, J. A. (1990) *J. Biochem. Biophys. Methods 21*, 35−46.

Belikova, Y. O., Burov, V. I., & Vinogradov, A. D. (1988) *Biochim. Biophys. Acta 936*, 10−19.

Bernasconi, C. F. (1976) in *Relaxation Kinetics*, Academic Press, New York.

Bisswanger, H., Kirschner, K., Cohn, W., Hager, V., & Hansson, E. (1979) *Biochemistry 18*, 5946−5953.

Braus, G. H., Luger, K., Paravicini, G., Schmidheini, T., Kirschner, K., & Hütter, R. (1988) *J. Biol. Chem. 263*, 7868−7875.

Cohn, W., Kirschner, K., & Paul, C. (1979) *Biochemistry 18*, 5953−5959.

Crawford, I. P. (1989) *Annu. Rev. Microbiol. 43*, 567−600.

Creighton, T. E. (1968) *J. Biol. Chem. 243*, 5605−5609.

Creighton, T. E. (1970) *Biochem. J. 120*, 699−707.

Creighton, T. E., & Yanofsky, C. (1970) *Methods Enzymol. 17a*, 365−380.

Cunningham, E. B. (1978) *Biochemistry*: *Mechanisms of Metabolism*, pp 717−723, McGraw Hill, New York.

Doy, C. H. (1966) *Nature (London) 211*, 736−737.

Doy, C. H., & Gibson, F. (1959) *Biochem. J. 72*, 586−597.

Duggleby, R. G., & Morrison, J. F. (1977) *Biochim. Biophys. Acta 481*, 297−312.

Eberhard, M. (1990a) Ph.D. Dissertation, University of Basel, Basel, Switzerland.

Eberhard, M. (1990b) *CABIOS 6*, 213−221.

Eberhard, M., Tsai-Pfugfelder, M., Bolewska, K., Hommel, U., & Kirschner, K. (1995) *Biochemistry 34*, 5419−5428.

Eisenthal, R., & Cornish-Bowden, A. (1974) *Biochem. J. 139*, 715−720.

Farber, G. K., & Petsko, G. A. (1990) *Trends Biochem. Sci. 15*, 228−234.

Fernley, H. N. (1974) *Eur. J. Biochem. 43*, 377−378.

Hankins, C. N., Largen, M., & Mills, S. E. (1975) *Anal. Biochem. 69*, 510−517.

Harayama, S., & Rekik, M. (1990) *Mol. Gen. Genet. 221*, 113−120.

Hiromi, K. (1978) in *Kinetics of Fast Enzyme Reactions: Theory and Practice*, Kodansha Scientific Ltd., Tokyo.

Hommel, U., Lustig, A., & Kirschner, K. (1989) *Eur. J. Biochem. 180*, 33−40.

Isbell, H. S., & Frush, H. L. (1958) *J. Org. Chem. 23*, 1309−1319.

Kirschner, K., Szadkowski, H., Henschen, A., & Lottspeich, F. (1980) *J. Mol. Biol. 143*, 395−409.

Kirschner, K., Szadkowski, H., Jardetzky, T. S., & Hager, V. (1987) *Methods Enzymol. 142*, 386−397.

Luger, K., Hommel, U., Herold, M., Hofsteenge, J., & Kirschner, K. (1989) *Science 243*, 206−210.

Marquardt, D. W. (1963) *J. Soc. Ind. Appl. Math. 11*, 431−441.

Nimmo, I. A., & Atkins, G. L. (1974) *Biochem. J. 141*, 913−914.

Paul, C., Kirschner, K., & Haenisch, G. (1980) *Anal. Biochem. 101*, 442−448.

Pfugfelder, M. (1986) Ph.D. Dissertation, University of Basel, Basel, Switzerland.

Priestle, J. P., Grütter, M. G., White, J. L., Vincent, M. G., Kania, M., Wilson, E., Jardetzky, T. S., Kirschner, K., & Jansonius, J. N. (1987) *Proc. Natl. Acad. Sci. U.S.A. 84*, 5690−5694.

Schendel, F. J., Cheng, Y. S., Otvos, J. D., Wehrli, S., & Stubbe, J. (1988) *Biochemistry 27*, 2614−2623.

Stroud, R. M. (1994) *Nature Struct. Biol. 1*, 131−134.

Sugamaran, M., Semensi, V., Dali, H., & Saul, S. (1989) *FEBS Lett. 255*, 345−349.

Walsh, C. (1979) in *Enzymatic Reaction Mechanisms*, Freeman, San Francisco.

Wilmanns, M., Hyde, C. C., Davies, R. D., Kirschner, K., & Jansonius, J. N. (1991) *Biochemistry 30*, 9161−9169.

Wilmanns, M., Priestle, J. P., Niermann, T., & Jansonius, J. N. (1992) *J. Mol. Biol. 223*, 477−507.

BI941805K